UC Irvine
UC Irvine Previously Published Works

Title

Phase-resolved functional optical coherence tomography: simultaneous imaging of in situ tissue structure, blood flow velocity, standard deviation, birefringence, and Stokes vectors in human skin.

Permalink

https://escholarship.org/uc/item/0sx2h6pk

Journal

Optics Letters, 27(19)

ISSN

0146-9592

Authors

Ren, Hongwu
Ding, Zhihua
Zhao, Yonghua
et al.

Publication Date

2002-10-01

DOI

10.1364/ol.27.001702

Copyright Information

Peer reviewed

Phase-resolved functional optical coherence tomography: simultaneous imaging of *in situ* tissue structure, blood flow velocity, standard deviation, birefringence, and Stokes vectors in human skin

Hongwu Ren, Zhihua Ding, Yonghua Zhao, Jianjun Miao, J. Stuart Nelson, and Zhongping Chen

Beckman Laser Institute and Departments of Biomedical Engineering and Surgery, University of California, Irvine, California 92612

We describe a phase-resolved functional optical coherence tomography system that can simultaneously yield *in situ* images of tissue structure, blood flow velocity, standard deviation, birefringence, and the Stokes vectors in human skin. Multifunctional images were obtained by processing of analytical interference fringe signals derived from two perpendicular polarization-detection channels. The blood flow velocity and standard deviation images were obtained by comparison of the phases from pairs of analytical signals in neighboring A-lines in the same polarization state. The analytical signals from two polarization-diversity detection channels were used to determine the four Stokes vectors for four reference polarization states. From the four Stokes vectors, the birefringence image, which is not sensitive to the orientation of the optical axis in the sample, was obtained. Multifunctional *in situ* images of a port wine stain birthmark in human skin are presented. © 2002 Optical Society of America

OCIS code: 170.4500.

Optical coherence tomography (OCT) is a noninvasive, noncontact imaging modality that uses coherence gating to obtain high-resolution cross-sectional images of tissue microstructure.[1,2] OCT is analogous to ultrasound imaging, except that infrared light waves rather than acoustic waves are used. Consequently, the spatial resolution of OCT is more than an order of magnitude higher than that of ultrasound. Several extensions of OCT have been developed for functional imaging of tissue physiology. Optical Doppler tomography combines the Doppler principle with coherence gating for tomographic imaging of tissue microstructure and blood flow simultaneously.[3–5] Polarization-sensitive OCT combines polarization-sensitive detection with OCT to determine tissue birefringence.[6,7] Both techniques use phase information from the interference fringes to yield physiologically important information.[7–10] Although several potential clinical applications have been demonstrated, to date, optical Doppler tomography and polarization-sensitive OCT imaging have been performed with separate systems. However, there are many clinical indications where determination of both blood perfusion and tissue birefringence is important. For example, the loss of cutaneous blood perfusion and changes in tissue birefringence are two critical factors used to determine burn depth. Simultaneous imaging of the changes in blood perfusion and collagen birefringence by functional optical coherence tomography (F-OCT) may permit better clinical management of burn injuries.

In this Letter we describe a phase-resolved F-OCT system that can simultaneously obtain *in situ* images of tissue structure, blood flow velocity, standard deviation, and birefringence, and Stokes vectors in human skin. The system is based on a phase-resolved signal processing method whereby the multifunctional images are obtained from the

analytical interference fringe signals derived from two perpendicular polarization-detection channels. A fiber-based high-speed F-OCT system for multifunctional imaging is shown in Fig. 1. A 1.3-μm partially coherent light source with a bandwidth of 80 nm is used. Light entering a 2×2 fiber splitter is divided equally into the sample and reference arms of a Michelson interferometer. In the reference arm, a rapid-scanning optical delay line is aligned such that only group-delay scanning at 500 Hz is
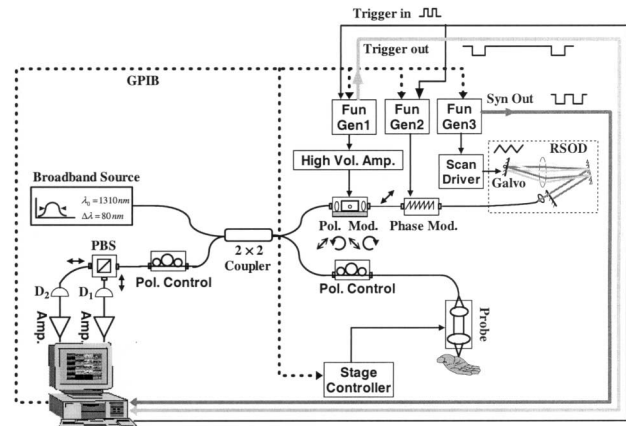

Fig. 1. Fiber-based F-OCT system. Pol. Mod., polarization-state modulator; Pol. Control; polarization controller; Phase Mod., phase modulator; PBS, polarization beam splitter; RSOD, rapid-scanning optical delay line; D_1, D_2, detectors; Galvo, galvanometer scanner; High Vol. Amp., high-voltage amplifier; Fun Gen1–Fun Gen3, function generators; Amp, low-noise preamplifier; GPIB, general-purpose interface bus; Syn Out, synchronizing signal of the driving signal for the galvanometer scanner, which is from Fun Gen3; Trigger in, trigger-in signal to Fun Gen1 and 2, which is generated from the analog-to-digital board; Trigger out, trigger-out signal from Fun Gen1 to arm the analog-to-digital board.

generated without phase modulation. A stable phase modulation at 500 kHz is generated with an electro-optic modulator for heterodyne detection.[9] The fringe signals from two polarization channels are detected by two photodetectors, high-pass filtered, amplified, and digitized by a dual-channel, 5-MHz, 12-bit analog-to-digital conversion board. A polarization modulator is used to control the polarization state of light in the reference arm, which varies rapidly between states that are orthogonal in the Poincaré sphere at 125 Hz. The choice of orthogonal polarization states in the Poincaré sphere is important because it ensures that the birefringence measurements will be independent of the orientation of the optical axis in the sample. The Stokes vectors, are accurately measured by generation of four states of light polarization for each lateral location. For each polarization state, four A-line scans are performed sequentially. Therefore, a total of 16 A-line scans are used to obtain images of tissue structure, Doppler mean frequency shift, Doppler standard deviation, phase retardation, and Stokes vectors simultaneously. A synchronizing time-clock diagram is shown in Fig. 2. Because Doppler- and polarization-sensitive detection requires phase information, we first calculate the complex analytical signal $\tilde{\Gamma}(t)$ of the interference fringe, using the Hilbert transformation[8]:

$$\tilde{\Gamma}(t) = 2 \int_0^\infty \int_0^\tau \Gamma(t')\exp(-2\pi i \nu t')\mathrm{d}t' \ \exp(2\pi i \nu t)\mathrm{d}\nu, \tag{1}$$

where τ is the time duration of the fringe signal in each axial scan.

For each polarization state, four sequential A-scans are performed. The Doppler frequency shifts (f_n) and standard deviation (σ_n) values at the nth pixel can be calculated with complex analytical signals from the four sequential A-scans[9,10]:

$$f_n = \frac{1}{2\pi T} \ \tan^{-1}\left\{\mathrm{Im}\left[\sum_{m=(n-1)M}^{nM}\sum_{j=1}^4 \tilde{\Gamma}_j(t_m)\tilde{\Gamma}_{j+1}^*(t_m)\right]\middle/\right.$$

$$\left.\mathrm{Re}\left[\sum_{m=(n-1)M}^{nM}\sum_{j=1}^4 \tilde{\Gamma}_j(t_m)\tilde{\Gamma}_{j+1}^*(t_m)\right]\right\}, \tag{2}$$

$$\sigma_n^2 = \frac{1}{2\pi^2 T^2}\left[1 - \frac{\left|\sum\limits_{m=(n-1)M}^{nM}\sum\limits_{j=1}^4 \tilde{\Gamma}_j(t_m)\tilde{\Gamma}_{j+1}^*(t_m)\right|}{\sum\limits_{m=(n-1)M}^{nM}\sum\limits_{j=1}^4 \langle\tilde{\Gamma}_j(t_m)\tilde{\Gamma}_j^*(t_m)\rangle}\right], \tag{3}$$

$\langle\tilde{\Gamma}_j(t_m)\tilde{\Gamma}_j^*(t_m)\rangle = \frac{1}{2}[\tilde{\Gamma}_j(t_m)\tilde{\Gamma}_j^*(t_m) + \tilde{\Gamma}_{j+1}(t_m)\tilde{\Gamma}_{j+1}^*(t_m)]$, where $\tilde{\Gamma}_j(t_m)$ and $\tilde{\Gamma}_j^*(t_m)$ are the complex signals at axial time t_m, corresponding to the jth A-scan and its conjugate, respectively, T is the time duration between A-scans, and M is an even number that denotes the window size in the axial direction for each pixel. Note

that Eq. (5) is slightly different from our previously published work.[10] We replaced term $\tilde{\Gamma}_j(t_m)\tilde{\Gamma}_j^*(t_m)$ with $1/2[\tilde{\Gamma}_j(t_m)\tilde{\Gamma}_j^*(t_m) + \tilde{\Gamma}_{j+1}(t_m)\tilde{\Gamma}_{j+1}^*(t_m)]$ to ensure nonnegativity in the variance values. The modified algorithm presented above also effectively reduces speckle noise. The calculated Doppler frequency shifts and standard deviation values for four polarization states are then averaged to yield the Doppler shift and variance images. The velocity sensitivity of phase-resolved F-OCT is ~10 μm/s. The Doppler flow image in phase-resolved F-OCT is very sensitive to any environmental disturbances such as sample stability. However, because we are interested in relative motion of blood flow with respect to tissue, we correct motion artifacts by choosing tissue as a stable reference point for phase measurement in each axial scan.[12]

For every polarization state controlled by the polarization modulator, A-scan signals corresponding to two orthogonal polarization diversity channels were digitized. The Stokes vector for the nth pixel can be derived from the analytical signal from two orthogonal polarization channels[7]:

$$S_{0,n} = \sum_{m=(n-1)M}^{nM}\sum_{j=1}^4 [\tilde{\Gamma}_j^H(t_m)\tilde{\Gamma}_j^{H^*}(t_m) + \tilde{\Gamma}_j^V(t_m)\tilde{\Gamma}_j^{V^*}(t_m)],$$

$$S_{1,n} = S_{0,n}^{-1}\sum_{m=(n-1)M}^{nM}\sum_{j=1}^4 [\tilde{\Gamma}_j^H(t_m)\tilde{\Gamma}_j^{H^*}(t_m)$$
$$- \tilde{\Gamma}_j^V(t_m)\tilde{\Gamma}_j^{V^*}(t_m)],$$

$$S_{2,n} = S_{0,n}^{-1}\sum_{m=(n-1)M}^{nM}\sum_{j=1}^4 2\,\mathrm{Re}[\tilde{\Gamma}_j^H(t_m)\tilde{\Gamma}_j^{V^*}(t_m)],$$

$$S_{3,n} = S_{0,n}^{-1}\sum_{m=(n-1)M}^{nM}\sum_{j=1}^4 2\,\mathrm{Im}[\tilde{\Gamma}_j^{H^*}(t_m)\tilde{\Gamma}_j^V(t_m)], \tag{4}$$

where S_0, S_1, S_2, and S_3 are the four components of the Stokes vector. S_1, S_2, and S_3 are the normalized coordinates of the Stokes vector in the Poincaré sphere that characterize the polarization state of the backscattered light, S_0 is the module of the Stokes vector characterizing light intensity, $\tilde{\Gamma}_j^H(t_m)$ and $\tilde{\Gamma}_j^V(t_m)$ are the complex signals detected from the two orthogonal polarization channels at axial time t_m, for the jth A-scan, and $\tilde{\Gamma}_j^{H^*}(t_m)$ and $\tilde{\Gamma}_j^{V^*}(t_m)$ are their conjugates. From the Stokes vectors for the four states of light polarization, the structural image is obtained by averaging of the four S_0. The phase-retardation image, which characterizes the birefringence distribution in the sample, is calculated by rotation of the Stokes vectors in the Poincaré sphere.[7]

Our phase-resolved F-OCT system was used to perform *in situ* imaging of a port wine stain birthmark in human skin. Simultaneous imaging of tissue structure, blood flow velocity, standard deviation, birefringence, and the Stokes vectors is shown in Fig. 3. The image area is 2 mm × 1.5 mm, with 200 × 150 pixels and 3200 axial scans. With a 500-Hz axial scanner in the delay line, the image acquisition time is approximately 7 s. Image acquisition times of less
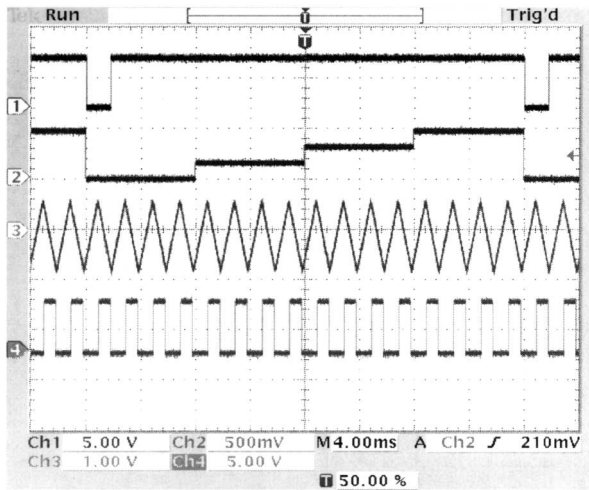
Fig. 2.   Synchronizing time-clock diagram for the F-OCT system.   Channel (Ch) 1 is the signal generated from the synchronized trigger output of function generator 1 and arms the analog-to-digital conversion.   Channel 2 is the signal generated by function generator 1 to control the polarization modulator.   Channel 3 is the triangle signal from the function generator 3 to control the galvanometer scanning.   Channel 4 is the signal generated by synchronized output of function generator 3 through a digital delay.   This signal is used to trigger the phase modulation and data acquisition.
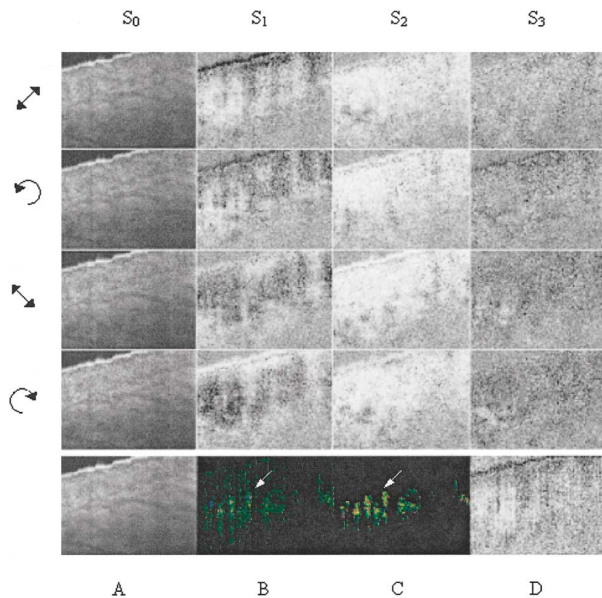

Fig. 3.   Simultaneous imaging of the Stokes vectors, structure, blood flow velocity, standard deviation, and birefringence from *in vivo* human skin.   The top four panels are the Stokes vector image corresponding to the four reference polarization states.   The bottom four panel images are A, structural image; B, blood flow velocity image; C, standard deviation image; D, phase-retardation image.

than 1 s are possible if an 8-kHz resonator scanner is used.   The computation time to derive all the images with a Pentium IV PC is less than 10 s.   The top four panels are the Stokes vectors corresponding to the four different polarization states shown in Fig. 2.   From left to right, they are S_0, S_1, S_2, and S_3, obtained by averaging of four A-lines in every polarization

state.   The bottom panel images are tissue structure, Doppler frequency shift (blood flow velocity), standard deviation, and birefringence.   Implementation of the polarization-diveristy detection in the intensity, Doppler and standard deviation images significantly reduces the artifact due to tissue birefringence.   In addition, speckle noise is also greatly reduced.   The greater detail noted in the structural image compared with the S_0 image indicates that the speckle noise is greatly reduced when polarization-diversity detection is used and multiple scans are averaged.   Small vessels can be clearly identified in the Doppler frequency shift and standard deviation images.   The arrows in the Doppler frequency shift and standard deviation images indicate that the blood vessels are located approximately 500 μm below the skin surface.   The nonuniform birefringence of human skin can also be identified in the phase-retardation image.

In summary, we have developed a phase-resolved F-OCT system capable of simultaneous imaging of *in situ* tissue structure, blood flow velocity, standard deviation, birefringence, and the Stokes vectors in human skin.

References

1. D. Huang, E. A. Swanson, C. P. Lin, J. S. Schuman, W. G. Stinson, W. Chang, M. R. Hee, T. Flotte, K. Gregory, C. A. Puliafito, and J. G. Fujimoto, Science **254,** 1178 (1991).
2. B. E. Bouma and G. J. Tearney, *Handbook of Optical Coherence Tomography* (Marcel Dekker, New York, 2002).
3. Z. Chen, T. E. Milner, D. Dave, and J. S. Nelson, Opt. Lett. **22,** 64 (1997).
4. Z. Chen, T. E. Milner, S. Srinivas, X. J. Wang, A. Malekafzali, M. J. C. van Gemert, and J. S. Nelson, Opt. Lett. **22,** 1119 (1997).
5. J. A. Izatt, M. D. Kulkarni, S. Yazdanfar, J. K. Barton, and A. J. Welch, Opt. Lett. **22,** 1439 (1997).
6. M. R. Hee, D. Huang, E. A. Swanson, and J. G. Fujimoto, J. Opt. Soc. Am. B **9,** 903 (1992).
7. C. E. Saxer, J. F. de Boer, B. H. Park, Y. Zhao, Z. Chen, and J. S. Nelson, Opt. Lett. **25,** 1355 (2000).
8. Z. Chen, Y. Zhao, S. M. Srinivas, J. S. Nelson, N. Prakash, and R. D. Frostig, IEEE J. Sel. Topics Quantum Electron. **5,** 1134 (1999).
9. Y. Zhao, Z. Chen, C. Saxer, S. Xiang, J. F. de Boer, and J. S. Nelson, Opt. Lett. **25,** 114 (2000).
10. Y. Zhao, Z. Chen, C. Saxer, Q. Shen, S. Xiang, J. F. de Boer, and J. S. Nelson, Opt. Lett. **25,** 1358 (2000).
11. Z. Ding, Y. Zhao, H. Ren, S. J. Nelson, and Z. Chen, Opt. Express **10,** 236 (2002), http://www.opticsexpress.org.
12. Y. Zhao, Z. Chen, Z. Ding, H. Ren, and J. S. Nelson, IEEE J. Sel. Topics Quantum Electron. **7,** 931 (2001).